HHS Public Access

Author manuscript

Curr Biol. Author manuscript; available in PMC 2017 August 08.

Published in final edited form as:

Curr Biol. 2016 August 8; 26(15): 2052–2059. doi:10.1016/j.cub.2016.06.007.

Lamin mutations accelerate aging via defective export of mitochondrial mRNAs through nuclear envelope budding

Yihang Li, **Linda Hassinger**, **Travis Thomson**, **Baojin Ding**, **James Ashley**, **William Hassinger**, and **Vivian Budnik**

Department of Neurobiology, University of Massachusetts Medical School, Worcester, MA

SUMMARY

Defective RNA metabolism and transport are implicated in aging and degeneration[1, 2], but the underlying mechanisms remain poorly understood. A prevalent feature of aging is mitochondrial deterioration[3]. Here we link a novel mechanism for RNA export through nuclear envelope (NE) budding[4, 5] that requires A-type Lamin, an inner nuclear membrane-associated protein, to accelerated aging observed in *Drosophila* LaminC (LamC) mutations. These LamC mutations were modeled after A-Lamin (LMNA) mutations causing progeroid syndromes (PS) in humans. We identified *mitochondrial assembly regulatory factor* (*marf*), a mitochondrial fusion factor (mitofusin), as well as other transcripts required for mitochondrial integrity and function, in a screen for RNAs that exit the nucleus through NE-budding. PS-modeled LamC mutations induced premature aging in adult flight muscles, including decreased levels of specific mitochondrial protein transcripts (RNA) and progressive mitochondrial degradation. PS-modeled LamC mutations also induced the accelerated appearance of other phenotypes associated with aging, including a progressive accumulation of poly-ubiquitin aggregates[6, 7] and myofibril disorganization[8, 9]. Consistent with these observations, the mutants had progressive jumping and flight defects. Downregulating *marf* alone induced the above aging defects. Nevertheless, restoring *marf* was insufficient for rescuing the aging phenotypes in PS-modeled LamC mutations, as other mitochondrial RNAs are affected by inhibition of NE-budding. Analysis of NE-budding in dominant and recessive PS-modeled LamC mutations suggests a mechanism by which abnormal lamina organization prevents the egress of these RNAs via NE-budding. These studies connect defects in RNA export through NE-budding to progressive loss of mitochondrial integrity and premature aging.

eTOC Blurb

Correspondence to: Vivian Budnik.

AUTHOR CONTRIBUTIONS

Conceptualization: V.B., J.A. and Y.L.; Methodology: Y.L., V.B.; Validation: Y.L.; Investigation: Y.L., L.H., T.T., B.D., J.A., W.H.; Resources: V.B., Department of Neurobiology, UMMS Electron microscopy core; Formal analysis: Y.L., B.D., V.B.; Visualization: V.B.; Writing—Original draft: V.B., Writing—Review & editing: Y.L., J.A., V.B.; Project administration: Y.L., V.B.; Funding acquisition: V.B.; Supervision: V.B., J.A.

Li et al. link the nuclear envelope (NE) budding export pathway to premature aging in fly models of progeroid syndromes induced by A-type lamin mutations. They find mitochondrial RNAs, such as Mitofusin, at NE budding sites and show that disruption of NE budding prior to adulthood results in accelerated aging and mitochondrial degeneration in adults.

Keywords

Progeroid Syndrome (PS); Nuclear envelope budding; RNA Export; Aging; mitochondria; sarcopenia; Drosophila; Mitochondrial assembly regulatory factor (marf); ATP synthase

RESULTS AND DISCUSSION

Mitochondrial RNAs localize to NE-budding sites

NE-budding is a mechanism for the nuclear export of large ribonucleoprotein granules (megaRNPs)[4]. This mechanism is akin to the nuclear egress of Herpes-type viruses[10] and involves megaRNP envelopment at the inner nuclear membrane (INM), and RNP de-envelopment at the outer nuclear membrane (ONM). Sites of NE-budding in *Drosophila* larval muscle nuclei are identified by using antibodies to the C-terminal fragment of DFrizzled2 (DFz2C), which associates with megaRNPs, and by the presence of locally thickened NE with brighter LamC immunoreactivity (DFz2C/LamC foci)[4, 11]. These DFz2C/LamC foci are enriched in RNAs encoding for several postsynaptic proteins [4, 12]. Fluorescent *in situ* hybridization (FISH) demonstrated that a subset of LamC foci also contained *marf* RNA (Fig. 1A; Fig. S1A–B), implicating NE-budding in the export of mitochondria-related transcripts. RNA-immunoprecipitation (RIP) from larval muscles using anti-DFz2C established that *marf* RNA, but not the unrelated *mad* RNA[4], co-precipitated with DFz2C, consistent with its presence in megaRNPs (Fig. 1B).

To determine if other mitochondria-associated RNAs existed in megaRNPs, we performed FISH to detect ATP-synthase (ATP-syn) subunits, the electron-transport chain component COX4, the kinase PINK1, and the mitochondrial fission factor Drp1. *ATP-syn-β*, *-α (Bellweather/Blw)*, and *-B* RNAs were enriched at NE-LamC foci, suggesting their presence in megaRNPs (Fig. 1C–E; Fig. S1C–E). FISH signal for *ATP-syn-γ*, *-C*, and *Drp1* was very low (not shown) and undetected for *cox4* and *pink1* (Fig. 1F,G). Thus, only a subset of mitochondria-associated transcripts are present within megaRNPs.

PS-modeled LamC mutations display age-dependent mitochondrial defects

Marf, a GTPase of the mitofusin family, is involved in mitochondrial fusion, a process essential for maintaining mitochondrial integrity and respiratory function[13]. Similarly, ATP-synthase is required for the formation and maintenance of mitochondrial cristae[14]. As aging and neurodegenerative disorders have been linked to progressive mitochondrial disruption [8, 15], we examined mitochondria in flies expressing PS-modeled LamC mutations. These LamC variants contained point mutations in conserved amino acid codons that in human *LMNA* gave rise to PS (Fig. 1I). We focused on LamC-E174K (E159K in LMNA) and LamC-R564C (R527C in LMNA; referred to as LamC-r564c to denote recessive inheritance) in the rod and tail domains of LamC (Fig. 1I). We also generated flies

expressing wild-type LamC (LamC-WT). In humans LMNA-E159K is an autosomal-dominant mutation causing Atypical-PS with a presentation similar to Hutchinson Gilford Progeria Syndrome (HGPS)[16]. LMNA-r527c is an autosomal-recessive mutation inducing atypical-HGPS[17]. Western-blots of body wall muscle proteins from *lamC* null mutants expressing LamC variants with MHC-Gal4 revealed that the transgenes were expressed in the same range as wild-type (Fig. 1H). Since LMNA-E159K behaves as a dominant mutation in humans, LamC-E174K was expressed in a *lamC/+* heterozygous background (genotype: LamC-E174K, *lamC/+*). Since LMNA-r527c is a recessive mutation in humans, LamC-r564c, was expressed in a *lamC* mutant homozygous background (genotype: LamC-r564c, *lamC/lamC*).

We focused on adult dorsal longitudinal muscles (DLM) of the indirect flight-muscles, since larval muscles are short-lived, precluding aging studies[18]. We examined mitochondria using antibodies against mammalian ATP-syn-α, which cross-react with Blw[19], in young (3-day post eclosion; 3d) and middle age (14d and 21d) adults.

In wild-type and LamC-WT, anti-ATP-syn-α labeled elongated mitochondria located above and below myofibrils at all stages (Fig. 2A,D,G,B,E,H), which was similar to 3d LamC-E174K (Fig. 2C). In 14d and 21d LamC-E174K, however, mitochondria were smaller, appeared rounded, and were sparse (Fig. 2F,I). This was reflected by a significant reduction of mitochondrial volume (Fig. 2J), suggesting an age-dependent decline in mitochondria production and/or maintenance. *lamC* null mutants did not survive to adulthood, precluding the examination of animals expressing LamC-r564c.

These mitochondrial phenotypes and the presence of *marf* RNA in megaRNPs raised the possibility that age-dependent mitochondrial deterioration could be partially attributed to defective Marf levels. Indeed, *marf* RNA was markedly depleted in thoracic muscles from 21d LamC-E174K, compared to 21d controls and LamC-WT (Fig. 2K).

At the ultrastructural level, in 4d and 21d controls, mitochondria were packed between myofibrils, which was maintained even in 60d animals (Fig. 3A; Fig. S2A1,D1). This was similar to 4d and 21d LamC-WT (Fig. S2B1,E1), and 4d LamC-E174K (Fig. S2C1). Additionally, mitochondrial cristae appeared normal (Fig. 3A; Fig. S2A2,B2,D2,E2). Instead, 14d and 21d LamC-E174K animals exhibited swollen mitochondria (Fig. 3B,C), with collapsing or disintegrating cristae (Fig. 3B,C). This was reflected in a significant reduction in mitochondria electron density (Fig. S2F). Closer examination already revealed subtle abnormalities in 4d LamC-E174K animals (Fig. S2C2).

Expression of Marf-RNAi in DLMs also elicited dramatic mitochondrial aberrations (Fig. 3D,E; Fig. S2F). However, overexpressing Marf in the DLM of LamC-E174K, *lamC/+* animals was insufficient to rescue mitochondrial defects (Fig. 2J,L; Fig. 3G; Fig. S2F). Thus, Marf is not the only mitochondrial factor involved in maintaining mitochondrial integrity in PS-LamC mutations. Indeed, downregulating the megaRNP component, Blw, also elicited mitochondrial defects (Fig. 3F; Fig. S2F).

To determine if the mitochondrial phenotypes resulted from defective NE-budding and not NPC-mediated export[20], we expressed DFz2-dominant-negative (DFz2-DN)[21], a LamC-

independent method to block NE-budding. This induced mitochondrial disruption, including sparse and collapsed cristae (Fig. 3H; Fig. S2F).

We also observed progressive defects in muscle fibers in LamC-E174K animals. In contrast to controls, LamC-WT, and 4d LamCE174K (Fig. S3A–G), 21d LamCE174K animals exhibited thinner myofibrils, sarcomere disorganization, and vanishing Z-lines and A-bands (Fig. S3H), consistent with the sarcopenia observed in very old wild-type flies. This phenotype was mimicked by expressing Marf-RNAi in DLMs (Fig. S3I).

PS-modeled LamC mutations display additional signs of aging

An aging marker is a decline in protein quality control, resulting in accumulation of poly-ubiquitinated protein aggregates[6, 7]. In 3d, 14d, and 21d-day old wild-type flies we observed no poly-ubiquitin aggregates in DLMs (Fig. S3J–K,M), but these were abundant in 60-day old flies (Fig. S3L,M).

DLMs from 3d LamC-WT or LamC-E174K flies were devoid of poly-ubiquitin aggregates (Fig. 3I,J,O). However, numerous poly-ubiquitin aggregates were observed in 14d LamC-E174K, but not LamC-WT flies (Fig. 3K,L,P). Thus, LamC-E174K animals display accelerated defects in proteostasis, as in normal aging. Downregulating Marf in muscle also led to early appearance of poly-ubiquitin aggregates (Fig. 3M,P), and overexpressing Marf in LamC-E174K DLMs partially rescued levels of poly-ubiquitin aggregates (Fig. 3N,P). Given that expressing LamC-E174K leads to a reduction in Marf, and that downregulating Marf alone mimics LamC-E174K phenotypes, these results provide compelling evidence for a primary role of Marf in sustaining mitochondrial integrity, normal muscle mass and proteostasis. Lack of proper mitochondrial replenishment leads to reactive oxygen species (ROS) accumulation in mitochondria derived from oxidative metabolism, inducing cellular damage. Indeed, HGPS patients display an increase in ROS, altered energy generation, and elevated genomic instability markers[22]. Our studies raise the possibility that at least some of the defects observed in PS are derived from abnormal transport of RNAs that are required to sustain mitochondrial replenishment.

Mitochondrial replenishment is based on an equilibrium among mitochondrial fusion, fission and autophagy. Balanced mitochondrial fusion and fission restores damaged mitochondrial compartments, while excessive fission leads to fragmentation followed by autophagy to dispose of damaged mitochondria. Studies suggest that normal aging is accompanied by a shift towards fission and decreased fusion[23]. Our studies indicate that a decrease in mitochondrial fusion might result from abnormal RNA export in PS-modeled mutations. Interestingly, we found that LamC-E174K induced a decrease in *marf*, accompanied by accelerated disruption of mitochondria. As *marf* RNA is a component of megaRNPs and LamC-E174K disrupts NE-budding (see below), these observations are consistent with a role of NE-budding in the export of mitochondrial factors required for normal aging.

MegaRNPs have been associated with developmental periods characterized by high protein synthesis demand, such as after fertilization of the mammalian oocyte and during the rapid expansion of the fly larval NMJ. Interestingly, *marf* RNA expression is moderate throughout development, with a peak near the end of embryogenesis, and a very large peak in the young

adult, starting at late pupariation and increasing into early adulthood (http://flybase.org/reports/FBgn0029870.html). The progressive deterioration of muscles and mitochondria observed in PS-modeled adults is consistent with a gradual run-down of mitochondrial components needed to be maintained at high levels in the adult. Flight-muscle function imposes great energy demands, making it likely that mitochondria in flight-muscles require continuous replenishment. It is thus conceivable that NE-budding serves to provide an early pool of the RNAs required to sustain this replenishment, and that blocking NE-budding dramatically decreases the size of this early pool. In turn, this leads to early aging, due at least in part to an inability to restore mitochondrial function, and thus the damaging effects of increased ROS.

LamC-E174K expression disrupts flight behavior

The abnormalities in middle-age LamC-E174K DLMs were reflected in flight and wing position defects. Unlike wild-type, LamC-WT and young LamC-E174K flies (Fig. 4A), 21d LamC-E174K animals had a “wings-up” wing position (Fig. 4B). Also, 21d LamC-E174K failed to jump or fly, as determined in a flight assay[24] conducted within an oil-coated cylinder. Wild-type, LamC-WT and 3d LamC-E174K flies jump and fly when startled, becoming stuck at various heights of the cylinder walls (Fig. 4C; Movie S1, S2). 21d LamC-E174K showed about a 50% decrease in landing height (Fig. 4C), resulting from an inability to jump and fly (Movie S2). Consistent with a role of Marf in the above defect, Marf downregulation in muscles also elicited similar behavioral defects (Fig. 4C).

PS-modeled LamC mutations have defective NE-budding

The observations above raised the possibility that defects in NE-budding could be linked to accelerated aging. Thus, we determined if PS-modeled LamC mutations elicited NE-budding defects prior to the aging defects, using 3 readouts: the presence of nuclear DFz2C/LamC foci, megaRNP granules at the perinuclear space, and the development of the larval NMJ, whose growth and maturation require the export of certain postsynaptic RNAs through NE-budding[4, 11].

LamC-WT larval muscle nuclei contained DFz2C/LamC foci that were similar to controls in appearance and number (Fig. 4D,F,G; arrows). In contrast, nuclei in LamC-E174K larvae displayed dramatic decrease in DFz2C/LamC foci (Fig. 4D,H). Instead, the lamina exhibited numerous small blebs which, except for rare occasions, were devoid of DFz2C (Fig. 4H,L; arrowheads; Fig. S4A). Such blebs are observed in wild-type at a very low frequency (Fig. 4F; arrowhead). Consistent with LamC-r564c behaving as a recessive mutation, LamC-r564c, *lamC*/+ heterozygotes did not display the above phenotypes (Fig. 4L). Nevertheless, when expressed in a *lamC* null background, LamC-r564c showed a significant decrease in DFz2C/LamC foci (Fig. 4E,K) and a copious increase in nuclear blebs (Fig. 4K,M; Fig. S4B–C). Blebs were not observed in controls, *lamC* nulls, or LamC-WT. (Fig. 4I,J,M). Similar lamina blebs were observed in *Drosophila* Schneider-2 (S2) cells upon induction of LamC variant expression (Fig. S4D–F). The disruption of DFz2C/LamC foci formation suggests defective NE-budding in PS-LamC mutations.

At the ultrastructural level, megaRNPs in control and LamC-WT cells/muscles were observed at the NE either as single (Fig. S4G) or clustered electron dense granule(s) at the perinuclear space (Fig. 4N)[4, 11]. These granules and associated NE represent the DFz2C/LamC foci observed by light microscopy[4]. Upon expressing LamC-E174K or LamC-r564c several common abnormalities were observed. First, megaRNPs were localized within aberrant blebs of the NE (Fig. 4O; white arrow; Fig. S4H,M,N). These blebs were limited by INM and ONM, and beneath the INM there were areas of irregular and highly thickened lamina (Fig. 4O,P; black arrows; Fig. S4K). Thus, unlike the perinuclear space localization of normal megaRNPs, these granules were present in the nucleoplasm (Fig. S4H,L). The thickened lamina was particularly prominent at the neck of the blebs (Fig. 4O black arrowhead; Fig. S4H,K), but also in networks surrounding small nucleoplasmic islands Fig. 4Q,R; Fig. S4J; black arrows). Additionally, blebs devoid of megaRNPs were observed at high frequency (Fig. 4P; white arrowheads). These blebs most likely correspond to the blebs observed at the light microscopy level. Thus, PS-modeled mutations in LamC induce defects in NE-budding. These blebs have been previously observed in HGPS cells[25], but their significance was unknown. We propose that they represent sites of aborted NE-budding.

The above phenotype differed form the defects in NE-budding observed in *torsin* mutants[11]. In *torsin* mutants megaRNP granules bud into the perinuclear space but remain tethered to the INM by a “neck”, as Torsin appears to be required in pinching off the INM-coated granule[11] (Fig. S4L). In contrast, megaRNPs in PS-modeled LamC mutations were not surrounded by INM and remained naked in the nucleoplasmic side of the projection (Fig. S4L). We propose that in PS-modeled mutations LamC forms a disrupted lamina network, preventing megaRNPs from accessing the INM to bud into the perinuclear space. Unlike *torsin* mutants where megaRNP granules accumulate at the perinuclear space, very few megaRNPs were observed in PS-modeled LamC mutations. As megaRNPs are tightly surrounded by INM in *torsin* mutants, it is possible that they are protected from degradation. Instead, megaRNPs in PS-modeled mutations remain in the nucleoplasm being susceptible to degradation. This is supported by the observation that *marf* RNA is severely decreased in the LamC mutations and does not simply accumulate in the nucleus.

PS-modeled LamC mutations impair NMJ development

As another NE-budding read-out we examined the larval NMJ. Mutations in genes encoding components of NE budding result in the accumulation of immature synaptic boutons (ghost boutons) that fail to recruit postsynaptic proteins[4, 11]. This phenotype can be visualized by labeling NMJs with markers of the presynaptic (anti-HRP) and postsynaptic (anti-DLG) compartments, as ghost boutons lack DLG. We found that LamC-WT rescued the increase in ghost boutons in *lamC* mutants (Fig. S4O–P,R). In contrast, neither LamC-E174K nor LamC-r564c rescued this defect (Fig. S4Q,R). Thus, expression of PS-modeled LamC variants results in abnormal NMJ development and mimics the effects of inhibiting NE-budding. NE-budding blockade was observed in the larva, which is well before any signs of aging were detected, suggesting that NE-budding defects were unlikely to be caused by accelerated aging. We propose that certain transcripts required for mitochondrial renewal, are delivered from the nucleus through NE-budding. Mutations blocking NE-budding are initially normal, but fail to maintain this cellular state, resulting in accelerated aging.

HGPS patients do not display signs of intellectual disability[26]. However, PS patients commonly have decreased NMJ performance[27], defects in the enteric nervous system[28], low-frequency conductive hearing loss, and peripheral neuropathy[29]. Thus, synaptic dysfunction in PS patients cannot be completely ruled out. Our studies reveal a new role for NE-budding in aging and provide a mechanism for premature aging in certain laminopathies.

METHODS

For detailed Methods see Supplemental Material

Molecular Biology

LamC clone LD31805 was mutagenized using site-directed mutagenesis. For fly transformation LamC constructs were subcloned into pUAST-attB.

Fly strains

pUAST-LamC-WT, pUAST-LamC-E174K and pUAST-LamC-R564C were integrated at P2(3L)68A4. Stocks used: CS (wild-type), UAS-Marf-RNAi, UAS-Blw-RNAi, UAS-Dfz2-DN, UAS-Marf-HA, $lamC^{EX296}$, $lamC^{EX265}$ and the Gal4 drivers BG487-Gal4 and MHC-Gal4.

Western Blots

Performed as in [30], with few modifications.

Immunocytochemistry

Performed in wandering 3rd instar body wall muscles, adult indirect flight-muscle thoraces, and S2 cells. Primary antibodies were anti-DLG_{PDZ}, anti-Ubiquitin-FK2, anti-LamC, anti-ATP5A, and anti-DFz2-C.

S2 cell culture

Generated and cultured as in[30]. Protein expression was induced with 0.7mM $CuSO_4$ for 24hr.

FISH

Performed as in[4], with few modifications.

Image acquisition, quantification and morphometric analysis

Performed as in[4]. Polyubiquitin and mitochondrial volume were normalized to muscle volume. Number of nuclear DFz2C/LamC foci, and percent of nuclei having more than 10 blebs, were determined from muscles 6 and 7 (A2, A3). Number of foci per nucleus was normalized to wild-type controls. Mitochondrial density was measured using ImageJ.

EM

Carried out as described in[4].

Flight Assay

Conducted as described in[24].

RIP

Performed as described in[12], with a few modifications.

qPCR

Performed as described in[12]. mRNA levels were calculated by the $2^{-\Delta Ct}$ method, where ΔCT = (DFz2C IP Ct − control IP Ct), and then normalized to Marf levels for RIP. For comparisons between genotypes, *marf* RNA levels were normalized to a reference gene, either *Ef1α48D* or *RpL32* [31] by the $2^{-\Delta Ct}$ method. RNA levels were then normalized to controls for each experiment.

Statistics

A one-way ANOVA followed by a Tukey *post-hoc* test was utilized for multiple comparisons.

Supplementary Material

Refer to Web version on PubMed Central for supplementary material.

Acknowledgments

We thank Dr. Lee Fradkin for helpful comments on the manuscript, as well as Dr. Melissa Moore and members of the Budnik lab for thoughtful discussions. We also thank the UMMS EM Facility for assistance in this project. We also thank Dr. Leo Pallanck for the UAS-Marf-HA line. Stocks obtained from the Bloomington Drosophila Stock Center (NIH P40OD018537) were used in this study. Supported by grant R01 NS063228 to VB.

References

1. Chandris P, Giannouli CC, Panayotou G, Kletsas D. Compromise in mRNA processing machinery in senescent human fibroblasts: implications for a novel potential role of Phospho-ATR (ser428). Biogerontology. 2010; 11:421–436. doi:410.1007/s10522-10010-19261-z. Epub 12010 Jan 10519. [PubMed: 20084458]
2. Cookson MR. Aging--RNA in development and disease. Wiley Interdiscip Rev RNA. 2012; 3:133–143. doi:110.1002/wrna.1109. Epub 2011 Sep 1006. [PubMed: 21898829]
3. Dupuis L. Mitochondrial quality control in neurodegenerative diseases. Biochimie. 2014; 100:177–83. Epub 2013 Aug 1016. DOI: 10.1016/j.biochi.2013.1007.1033 [PubMed: 23958438]
4. Speese SD, Ashley J, Jokhi V, Nunnari J, Barria R, Li Y, Ataman B, Koon A, Chang YT, Li Q, et al. Nuclear Envelope Budding Enables Large Ribonucleoprotein Particle Export during Synaptic Wnt Signaling. Cell. 2012; 149:832–846. [PubMed: 22579286]
5. Lee CP, Chen MR. Escape of herpesviruses from the nucleus. Rev Med Virol. 2010; 20:214–230. [PubMed: 20069615]
6. Demontis F, Perrimon N. FOXO/4E-BP signaling in Drosophila muscles regulates organism-wide proteostasis during aging. Cell. 2010; 143:813–825. doi:810.1016/j.cell.2010.1010.1007. [PubMed: 21111239]
7. Rubinsztein DC. The roles of intracellular protein-degradation pathways in neurodegeneration. Nature. 2006; 443:780–786. [PubMed: 17051204]

8. Demontis F, Piccirillo R, Goldberg AL, Perrimon N. Mechanisms of skeletal muscle aging: insights from Drosophila and mammalian models. Dis Model Mech. 2013; 6:1339–1352. doi:1310.1242/dmm.012559. Epub 012013 Oct 012552. [PubMed: 24092876]
9. Doran P, Donoghue P, O'Connell K, Gannon J, Ohlendieck K. Proteomics of skeletal muscle aging. Proteomics. 2009; 9:989–1003. doi:1010.1002/pmic.200800365. [PubMed: 19180535]
10. Mettenleiter TC, Muller F, Granzow H, Klupp BG. The way out: what we know and do not know about herpesvirus nuclear egress. Cell Microbiol. 2013; 15:170–178. doi:110.1111/cmi.12044. Epub 12012 Nov 12047. [PubMed: 23057731]
11. Jokhi V, Ashley J, Nunnari J, Noma A, Ito N, Wakabayashi-Ito N, Moore MJ, Budnik V. Torsin mediates primary envelopment of large ribonucleoprotein granules at the nuclear envelope. Cell Rep. 2013; 3:988–995. doi:910.1016/j.celrep.2013.1003.1015. Epub 2013 Apr 1011. [PubMed: 23583177]
12. Packard M, Jokhi V, Ding B, Ruiz-Canada C, Ashley J, Budnik V. Nucleus to Synapse Nesprin1 Railroad Tracks Direct Synapse Maturation through RNA Localization. Neuron. 2015; 86:1015–1028. doi:1010.1016/j.neuron.2015.1004.1006. Epub 2015 May 1017. [PubMed: 25959729]
13. Peterson CM, Johannsen DL, Ravussin E. Skeletal muscle mitochondria and aging: a review. J Aging Res. 2012; 2012:194821. Epub 192012 Jul 194819. doi: 10.1155/2012/194821 [PubMed: 22888430]
14. Davies KM, Anselmi C, Wittig I, Faraldo-Gomez JD, Kuhlbrandt W. Structure of the yeast F1Fo-ATP synthase dimer and its role in shaping the mitochondrial cristae. Proc Natl Acad Sci U S A. 2012; 109:13602–13607. doi:13610.11073/pnas.1204593109. Epub 1204592012 Aug 1204593103. [PubMed: 22864911]
15. Daum B, Walter A, Horst A, Osiewacz HD, Kuhlbrandt W. Age-dependent dissociation of ATP synthase dimers and loss of inner-membrane cristae in mitochondria. Proc Natl Acad Sci U S A. 2013; 110:15301–15306. doi:15310.11073/pnas.1305462110. Epub 1305462013 Sep 1305462114. [PubMed: 24006361]
16. Garg A, Subramanyam L, Agarwal AK, Simha V, Levine B, D'Apice MR, Novelli G, Crow Y. Atypical progeroid syndrome due to heterozygous missense LMNA mutations. J Clin Endocrinol Metab. 2009; 94:4971–4983. doi:4910.1210/jc.2009-0472. Epub 2009 Oct 4929. [PubMed: 19875478]
17. Liang L, Zhang H, Gu X. Homozygous LMNA mutation R527C in atypical Hutchinson-Gilford progeria syndrome: evidence for autosomal recessive inheritance. Acta Paediatr. 2009; 98:1365–1368. doi:1310.1111/j.1651-2227.2009.01324.x. Epub 02009 May 01326. [PubMed: 19432833]
18. Roy S, VijayRaghavan K. Muscle pattern diversification in Drosophila: the story of imaginal myogenesis. Bioessays. 1999; 21:486–498. [PubMed: 10402955]
19. Li L, Tian X, Zhu M, Bulgari D, Bohme MA, Goettfert F, Wichmann C, Sigrist SJ, Levitan ES, Wu C. Drosophila Syd-1, liprin-alpha, and protein phosphatase 2A B′ subunit Wrd function in a linear pathway to prevent ectopic accumulation of synaptic materials in distal axons. J Neurosci. 2014; 34:8474–8487. doi:8410.1523/JNEUROSCI.0409-8414.2014. [PubMed: 24948803]
20. Muchir A, van Engelen BG, Lammens M, Mislow JM, McNally E, Schwartz K, Bonne G. Nuclear envelope alterations in fibroblasts from LGMD1B patients carrying nonsense Y259X heterozygous or homozygous mutation in lamin A/C gene. Exp Cell Res. 2003; 291:352–362. [PubMed: 14644157]
21. Mathew D, Ataman B, Chen J, Zhang Y, Cumberledge S, Budnik V. Wingless signaling at synapses is through cleavage and nuclear import of receptor DFrizzled2. Science. 2005; 310:1344–1347. [PubMed: 16311339]
22. Mateos J, Landeira-Abia A, Fafian-Labora JA, Fernandez-Pernas P, Lesende-Rodriguez I, Fernandez-Puente P, Fernandez-Moreno M, Delmiro A, Martin MA, Blanco FJ, et al. iTRAQ-based analysis of progerin expression reveals mitochondrial dysfunction, reactive oxygen species accumulation and altered proteostasis. Stem Cell Res Ther. 2015; 6:119. doi:110.1186/s13287-13015-10110-13285. [PubMed: 26066325]
23. Scheckhuber CQ, Erjavec N, Tinazli A, Hamann A, Nystrom T, Osiewacz HD. Reducing mitochondrial fission results in increased life span and fitness of two fungal ageing models. Nat Cell Biol. 2007; 9:99–105. Epub 2006 Dec 2007. [PubMed: 17173038]

24. Benzer S. Genetic dissection of behavior. Sci Am. 1973; 229:24–37. [PubMed: 4202065]
25. Kandert S, Luke Y, Kleinhenz T, Neumann S, Lu W, Jaeger VM, Munck M, Wehnert M, Muller CR, Zhou Z, et al. Nesprin-2 giant safeguards nuclear envelope architecture in LMNA S143F progeria cells. Hum Mol Genet. 2007; 16:2944–2959. [PubMed: 17881656]
26. Nissan X, Blondel S, Navarro C, Maury Y, Denis C, Girard M, Martinat C, De Sandre-Giovannoli A, Levy N, Peschanski M. Unique preservation of neural cells in Hutchinson-Gilford progeria syndrome is due to the expression of the neural-specific miR-9 microRNA. Cell Rep. 2012; 2:1–9. Epub 2012 Jun 1021. DOI: 10.1016/j.celrep.2012.1005.1015 [PubMed: 22840390]
27. Greising SM, Call JA, Lund TC, Blazar BR, Tolar J, Lowe DA. Skeletal muscle contractile function and neuromuscular performance in Zmpste24 −/− mice, a murine model of human progeria. Age (Dordr). 2012; 34:805–819. doi:810.1007/s11357-11011-19281-x. Epub 12011 Jun 11329. [PubMed: 21713376]
28. Yang SH, Procaccia S, Jung HJ, Nobumori C, Tatar A, Tu Y, Bayguinov YR, Hwang SJ, Tran D, Ward SM, et al. Mice that express farnesylated versions of prelamin A in neurons develop achalasia. Hum Mol Genet. 2015; 24:2826–2840. doi:2810.1093/hmg/ddv2043. Epub 2015 Feb 2824. [PubMed: 25652409]
29. Goss JR, Stolz DB, Robinson AR, Zhang M, Arbujas N, Robbins PD, Glorioso JC, Niedernhofer LJ. Premature aging-related peripheral neuropathy in a mouse model of progeria. Mech Ageing Dev. 2011; 132:437–442. doi:410.1016/j.mad.2011.1004.1010. Epub 2011 May 1011. [PubMed: 21596054]
30. Koles K, Nunnari J, Korkut C, Barria R, Brewer C, Li Y, Leszyk J, Zhang B, Budnik V. Mechanism of evenness interrupted (evi)-exosome release at synaptic boutons. J Biol Chem. 2012; 287:16820–16834. [PubMed: 22437826]
31. Ling D, Salvaterra PM. Robust RT-qPCR data normalization: validation and selection of internal reference genes during post-experimental data analysis. PLoS One. 2011; 6:e17762. doi: 17710.11371/journal.pone.0017762. [PubMed: 21423626]

Highlights

- Mitochondrial RNAs, such as Mitofusin, localize to nuclear envelope budding sites
- A fly model of progeroid syndrome caused by A-type lamin mutations ages prematurely
- Aging phenotypes include mitochondrial degeneration and Mitofusin RNA depletion
- Accelerated aging phenotypes are preceded by a block of nuclear envelope budding

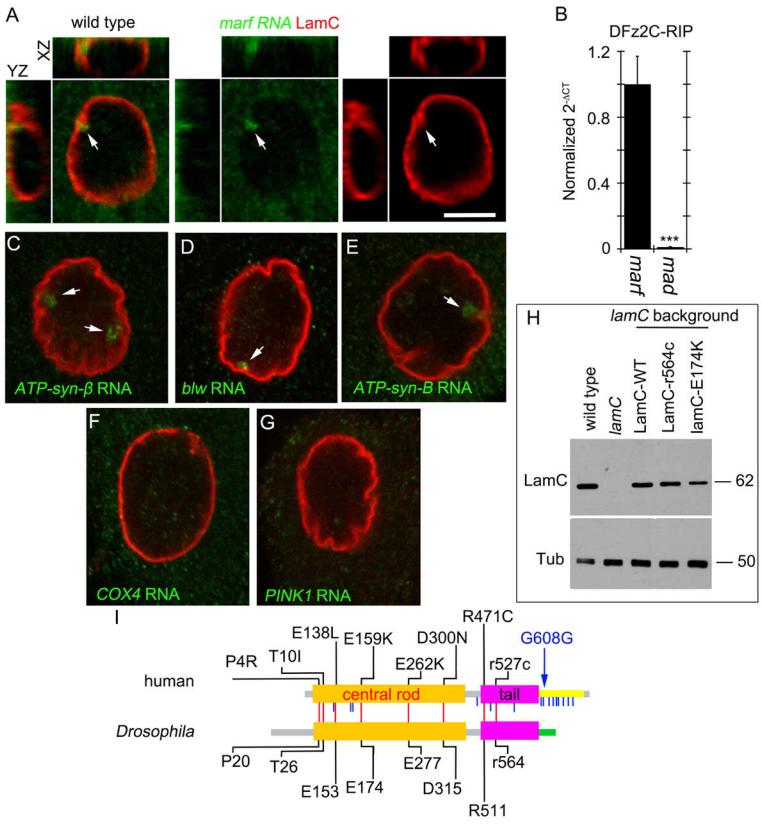

Figure 1. Association of *marf* mRNA with DFz2C and nuclear LamC foci

(see also Figure S1)

(**A, C–G**) FISH of a larval body wall muscle preparations using a (**A**) *marf* (**C**) *ATP-syn-β*, (**D**) *blw*, (**E**) ATP-syn-B, (**F**) *cox4*, (**G**) *pink1* DNA probe and antibodies to LamC. Arrows denote foci containing mitochondrial transcripts.

(**B**) Real time PCR of *marf* and *mad* after RNA-immunoprecipitation with DFz2C antibody from larval body wall muscles.

(**I**) Schematic depiction of *Drosophila* LamC and human LMNA protein structure, indicating conserved (red vertical lines) and non-conserved (blue vertical lines) amino acid residues that when mutated cause progeroid syndromes in humans. Blue arrow indicates the mutation responsible for most HGPS cases.

(**H**) Western blot of body wall muscle protein extracts from animals of the indicated genotypes probed with antibodies to LamC (top) and tubulin (Tub; bottom). Numbers at the right represent molecular weight in KDa.

***p<0.001 Error bars= SEM. Calibration bar in A, C–G is 6μm.

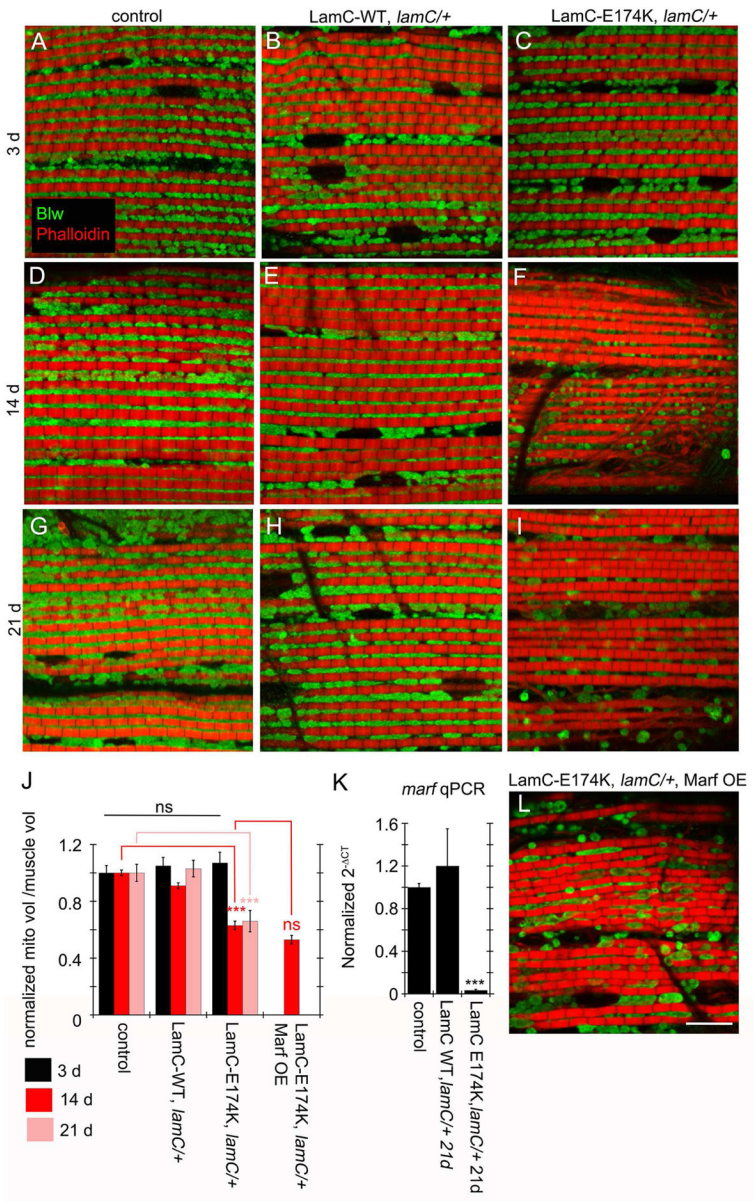

Figure 2. Age-dependent alterations in adult muscle mitochondria upon expressing LamC-E174K

(**A–I, L**) DLMs labeled with anti-ATP-syn-α and rhodamine-conjugated phalloidin from (**A–C**) 3- (**D–F L**) 14- and (**G–I**) 21-day old (**A,D,G**) MHC-Gal4 control; (**B,E,H**) LamC-WT, *lamC/+*; (**C,F,I**) LamC-E174K, *lamC/+* and (**L**) LamC-E174K, lamC/+, Marf OE

(**J**) Quantification of mitochondrial volume normalized to muscle volume.

(**K**) Real time PCR of *marf* RNA levels in adult thoracic muscle from the indicated genotypes.

N (left–right)= **J**: 30,49,28; 35,33,31; 28,47,32; 36. ***p< 0.001 Error bars= SEM. Calibration scale is 9μm.

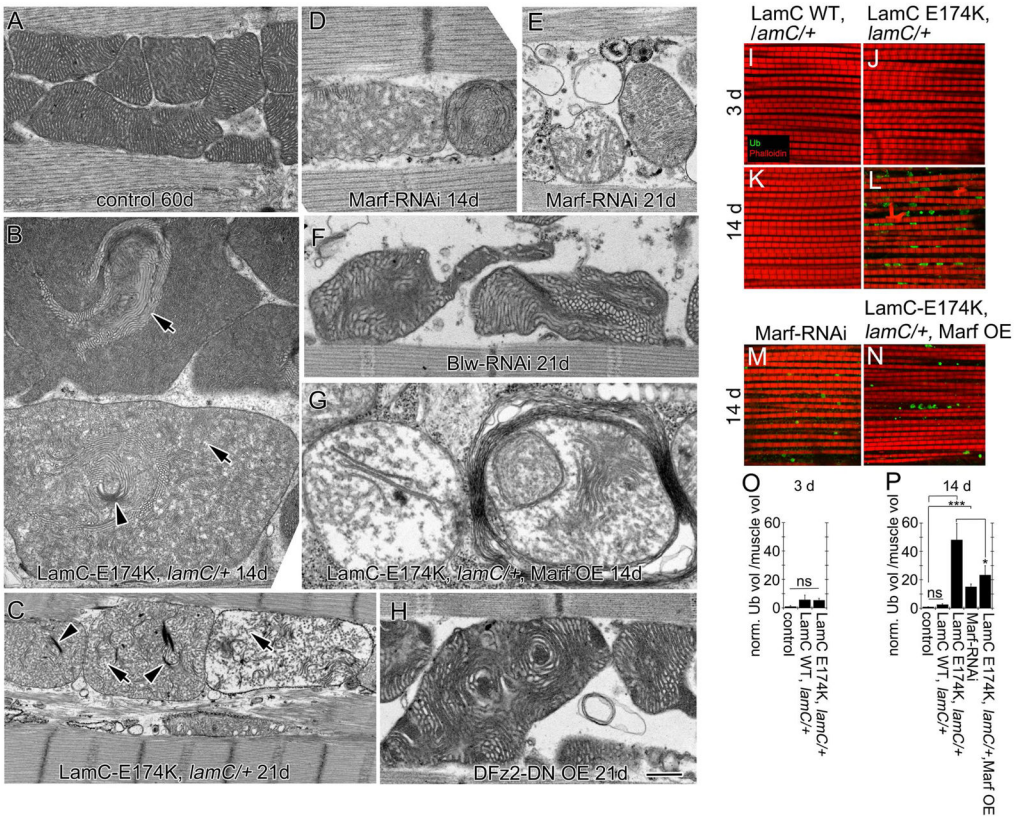

Figure 3. Disruption of adult muscle mitochondria and progressive polyubiquitin aggregate accumulation upon expressing LamC-E174K

(See also Figures S2 and S3)

(**A–H**) EM micrographs of adult DLMs showing mitochondrial cristae structure in (**A)** 60-day**, (B,D,G**) 14- and (**C,E,F,H**) 21-day old flies of the following genotypes: (**A)** MHC-Gal4/+, (**B,C**) LamC-E174K, *lamC/+*, (**D–E**) Marf-RNAi-muscle, (**F**) Blw-RNAi-muscle, (**G**) lamC-E174K, *lamC*/+ Marf OE, (**H**) DFz2-DN OE muscle. Arrowheads denote collapsing cristae; arrows denote disintegrating cristae.

(**I–N**) DLMs double labeled anti-ubiquitin and Rhodamine-conjugated phalloidin in (**I–J**) 3-, (**K–N**) 14-day old adults from (**I,K**) LamC-WT, *lamC/+*; (**J,L**) LamC-E174K, *lamC*/+; **(M)** Marf-RNAi-muscle and (**N**) LamC-E174K, *lamC*/+ Marf OE.

(**O–P**) Quantification of ubiquitin aggregate volume normalized to muscle volume.

N (left to right)= **O**: 29,30,29; **P**:85,30,35,36,36.

*p<0.05 ***p<0.001; Error bars= SEM

Calibration bar is 0.5μm for (A,B,H), 0.4μm for (D,E,F,G) , 1μm for (C) and 16μm for (I–N)

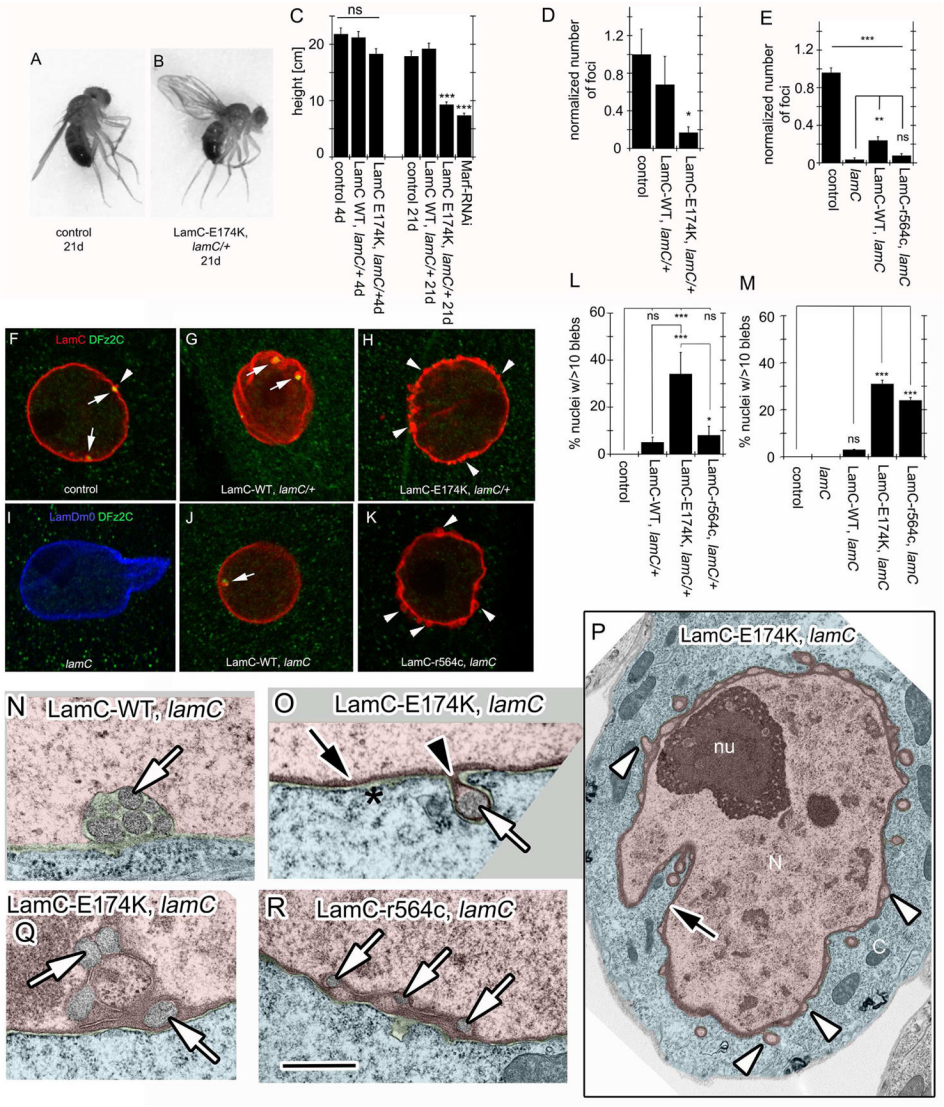

Figure 4. Expression of PS-modeled mutations disrupts NE morphology and ultrastructure
(see also Figure S4)

(**A–B**) Wing position in (**A**) control flies, showing normal wing position and (**B**) LamC-E174K, *lamC/+* flies showing a “wings up” phenotype.

(**C**) Quantification of landing height in 4- and 21-day old adults.

(**F–K**) Larval body wall muscle nuclei labeled with anti-LamC or anti-LamDm0, and anti-DFz2C antibody from (**F**) BG487-Gal4/+ control; (**G**) LamC-WT, *lamC*/+; Arrows denote LamC/DFz2C foci; Arrowheads denote abnormal LamC blebs. (**H**) LamC-E174K, *lamC*/+; (**I**) *lamC* null mutant; (**J**) LamC-WT, *lamC*; and (**K**) LamC-r564c, *lamC*. Arrows point to DFz2C/LamC foci, and arrowheads to blebs.

(**D,E**) Quantification of the number of DFz2C/LamC foci at body wall muscles normalized to BG487/+ controls in the indicated genotypes in a (**D**) *lamC/+* or (**E**) *lamC* null mutant background.

(**L,M**) Quantification of the percentage of body wall muscle nuclei containing more than 10 blebs at the NE in the indicated genotypes (**L**) in a *lamC/+* heterozygous background and (**M**) in a *lamC* null mutant background. Control is BG487/+ in both graphs.
(**N–R**) TEM of larval body wall muscle nuclei from (**N**) LamC-WT, *lamC*; (**O–Q**) LamC-E174K, *lamC*; and (**R**) LamC-r564c, *lamC*. White arrows denote megaRNP granules; White arrowheads denote empty blebs; Black arrows denote thickened lamina; Black arrowheads denote thickened lamina at the neck of blebs.
*p<0.05 **p<0.01 ***p<0.001 Error bars= SEM
N (left to right)= **C**: 81, 78, 83, 166, 83, 85, 89; **D**, **E**, **L**, **M**(number of hemisegments/ number of nuclei) **D**: 21/1137,21/1026,24/1248; **E**:17/958,13/666,17/951,19/977; **L**: 20/1155, 20/1106, 20/1035, 12/647; **M**:26/1500,14/720,23/1274,19/1079,16/829.
Calibration bar is 5.5μm for F–K, 1.4μm for P and 0.4μm for N, O, Q, R